Ion Permeation and Glutamate Residues Linked by Poisson-Nernst-Planck Theory in L-Type Calcium Channels

Wolfgang Nonner* and Bob Eisenberg#

*Department of Physiology and Biophysics, University of Miami School of Medicine, Miami, Florida 33101, and #Department of Molecular Biophysics and Physiology, Rush Medical College, Chicago, Illinois 60612, USA

ABSTRACT L-type Ca channels contain a cluster of four charged glutamate residues (EEEE locus), which seem essential for high Ca specificity. To understand how this highly charged structure might produce the currents and selectivity observed in this channel, a theory is needed that relates charge to current. We use an extended Poisson-Nernst-Planck (PNP2) theory to compute (mean) Coulombic interactions and thus to examine the role of the mean field electrostatic interactions in producing current and selectivity. The pore was modeled as a central cylinder with tapered atria; the cylinder (i.e., "pore proper") contained a uniform volume density of fixed charge equivalent to that of one to four carboxyl groups. The pore proper was assigned ion-specific, but spatially uniform, diffusion coefficients and excess chemical potentials. Thus electrostatic selection by valency was computed self-consistently, and selection by other features was also allowed. The five external parameters needed for a system of four ionic species (Na, Ca, Cl, and H) were determined analytically from published measurements of three limiting conductances and two critical ion concentrations, while treating the pore as a macroscopic ion-exchange system in equilibrium with a uniform bath solution. The extended PNP equations were solved with these parameters, and the predictions were compared to currents measured in a variety of solutions over a range of transmembrane voltages. The extended PNP theory accurately predicted current-voltage relations, anomalous mole fraction effects in the observed current, saturation effects of varied Ca and Na concentrations, and block by protons. Pore geometry, dielectric permittivity, and the number of carboxyl groups had only weak effects. The successful prediction of Ca fluxes in this paper demonstrates that ad hoc electrostatic parameters, multiple discrete binding sites, and logistic assumptions of single-file movement are all unnecessary for the prediction of permeation in Ca channels over a wide range of conditions. Further work is needed, however, to understand the atomic origin of the fixed charge, excess chemical potentials, and diffusion coefficients of the channel. The Appendix uses PNP2 theory to predict ionic currents for published "barrier-and-well" energy profiles of this channel.

INTRODUCTION

A single L-type Ca channel selectively admits $\sim 10^6$ Ca ions/s into a cell, even though only one in ~100 extracellular cations is calcium (reviewed by Tsien et al., 1987). Structural studies of this channel (Tanabe et al., 1987; Mikami et al., 1989) suggest that, as in other voltage-gated channels, the conduction properties of the open Ca channel are determined by small subdomains that line the ionic pathway in the form of hairpin folds. Each of the four internal repeats of the α_1-subunit of the channel contributes one hairpin subdomain to the pore, and each of these subdomains includes a glutamate residue in corresponding positions. These four glutamate residues (EEEE locus) are said to form the channel's selectivity filter because point mutations introduced at these positions alter the selectivity pattern of the channel (Yang et al., 1993; Kim et al., 1993; Mikala et al., 1993). Selectivity of Na channels appears to be controlled by an analogous DEKA locus, and mutations toward the EEEE pattern change Na channel selectivity toward the selectivity observed in Ca channels (Heinemann et al., 1992). The idea that a cluster of negatively charged structural groups is sufficient to establish a Ca channel-like selectivity is independently supported by the discovery that a mixed polymer, poly-3-hydroxybutyrate/polyphosphate, forms Ca-selective pores across planar lipid bilayers (Reusch et al., 1995; Das et al., 1997).

This paper is concerned with the question: To what extent, and how, can the selective conduction of calcium be attributed to Coulombic interactions between permeating ions and charged amino acid residues, such as glutamate carboxyl groups? Because Ca channels accept both monovalent and divalent cations, but with very different affinities (Hess et al., 1986), these channels likely use electrostatics in selecting their ion. An investigation of Ca channel electrostatics appears feasible, even with limited structural information, because Coulombic interactions usually occur over distances of many Ångstroms (Brooks et al., 1988, Chap. 3 and p. 172).

Previous quantitative approaches to Ca channel permeation have used descriptions at the thermodynamic level: an aqueous pore is said to transport ions by cycling through a sequence of hypothetical states distinguished by their patterns of ionic occupancy (Almers and McCleskey, 1984; Hess and Tsien, 1984; Dang and McCleskey, 1998). Free energies and transition rates associated with this process describe the pore and its contents as a thermodynamic entity (i.e., a black box). Because it is not clear how to proceed

Received for publication 14 January 1998 and in final form 27 May 1998.

Address reprint requests to Dr. Wolfgang Nonner, Department of Physiology and Biophysics, University of Miami School of Medicine, P.O. Box 016430, Miami, FL 33101. Tel.: 305-243-5536; Fax: 305-243-5931; E-mail: wnonner@chroma.med.miami.edu.

0006-3495/98/09/1287/19 $2.00

from the structure, or the charges, of the protein to predictions of flux, this kind of description is inadequate for analyzing the functional implications of internal structural elements.

Here we describe permeation as electrodiffusion (Nernst-Planck theory), with the Coulombic field computed by integration of Poisson's equation (Chen and Eisenberg, 1993; Eisenberg, 1996). Empirical parameters are used to represent ion-specific chemical affinities (Nonner et al., 1998) and friction. We consider a domain consisting of a cylindrical pore lined by charged groups, tapered atria, and hemispheres of bulk solution, and solve the Poisson-Nernst-Planck (PNP) equations in one dimension with approximate treatments of the atrial and bulk geometries. The bulk solutions contain four ionic species: Ca, Na, Cl, and protons.

Parameters for the PNP model are estimated analytically. The pore is assumed to function as a microscopic ion exchange column (Teorell, 1953; Helfferich, 1962) whose resin contains glutamate residues as charged groups. Macroscopic Donnan theory is applied to estimate five parameters that enable the resin to assume proper conductivities when it is equilibrated with solutions of certain compositions (e.g., a saturating Ca concentration). The resin parameters are inserted into the PNP model of the microscopic pore, and the system is solved numerically to predict Ca channel currents for nonequilibrium conditions.

The predicted currents exhibit properties strikingly similar to those observed in actual L-type Ca channels, including the shape of current/voltage relationships, reversal potentials, anomalous mole fraction behavior and proton block, as well as the saturation characteristics of Na and Ca currents. These features are predicted independently: none were used in the design of the model. Thus a PNP model based on crude structural information and five empirical parameters can accurately describe the interplay of Ca, Na, and hydrogen ions that determines the average current in the open Ca channel under a wide range of conditions.

The mean Coulombic field of the EEEE locus can account for about half of the channel's selective affinity for Ca over Na, because protonation of carboxyl groups limits the negative electric potential that can be created by the locus. This selectivity by valency thus must be complemented by other ion-specific interactions, which we describe here by excess chemical potentials. Interestingly, hypothetical channels with only one to three carboxyl groups are predicted to maintain about the same electric potential as a Ca channel with four carboxyls. The absolute conservation of the EEEE locus in Ca channels then suggests that glutamate residues are also involved in creating the excess chemical potentials that are needed for high Ca selectivity.

The Appendix examines barrier-and-well energy profiles for L-type Ca channels that have been proposed on the basis of rate-theory models of permeation (Almers and McCleskey, 1984; Hess and Tsien, 1984; Dang and McCleskey, 1998). When friction is considered and electrostatics are computed by solving Poisson's equation, the predicted currents that can flow across the proposed energy profiles are found to be inconsistent with those observed experimentally. The magnitude of conductances, ionic occupancies, and ionic selectivity are substantially different from those computed by rate theory. This indicates that the assumptions made in rate theory about electrostatics and friction (Hille and Schwarz, 1978) lead to unacceptable errors.

METHODS

The model described below (which we will call PNP2) extends in several respects the theory previously developed by Chen and Eisenberg (1993) (PNP0) and Eisenberg (1996). The extensions are (1) a chemical affinity to describe interactions between ions and pore that are not accounted for by the Coulombic force computed in PNP0 (PNP1) (Chen, 1997; Nonner, Chen and Eisenberg, 1998); 2) protonation of carboxyl groups lining the pore; 3) parameters that generally vary with position along the pore; and 4) an integration domain that extends from a narrow, cylindrical transmembrane pore into tapered atria and hemispherical bulk zones at both channel mouths. Because the PNP2 equations are solved over a domain that extends well into the bulk solutions, our computations include effects of current like diffusion polarization in the access and exit paths of the pore proper (Dani, 1986; Peskoff and Bers, 1988); concentrations and electric potentials at the boundaries of the extended domains are set to values found near the bath electrodes.

The Poisson-Nernst-Planck equations used for the Ca channel model describe the flux of ionic species k as a combination of diffusion and drift under an electrochemical force. They predict the current carried by ions (in all bath concentrations and at all membrane potentials) that interact with a channel with known diffusion coefficients $D(x)$, excess chemical potentials $\mu^0(x)$, and structural (i.e., fixed) charge $S(x)$:

$$J_k = -D_k(x)A(x)\left[\frac{dc_k(x)}{dx} + \frac{c_k(x)}{k_B T}\frac{d}{dx}(z_k e_0 V(x) + \mu_k^0(x))\right] \quad (1)$$

where the electric potential is given by Poisson's equation:

$$\epsilon_0\left[\epsilon(x)\frac{d^2V(x)}{dx^2} + \left(\frac{d\epsilon(x)}{dx} + \epsilon(x)\frac{d(\ln[A(x)])}{dx}\right)\frac{dV(x)}{dx}\right] = -\rho \quad (2)$$

The pore's net space charge density is

$$\rho = e_0 N_A[S(x) + \sum_k z_k C_k(x)] \quad (3)$$

The mean single-channel current and slope conductance contributed by all ions species k are

$$i = e_0 N_A \sum_k z_k J_k$$

$$\gamma = \frac{\partial i}{\partial V_m}$$

Slope conductances presented below have been estimated from finite differences of currents for voltage intervals of 5 mV centered about particular transmembrane voltages as indicated.

The symbols are as follows:

J_k	flux (per pore) of species k
x	position along pore axis
$D_k(x)$	position-dependent diffusion coefficient for species k
$A(x)$	position-dependent area of equipotential surface
$\mu_k^0(x)$	position-dependent excess chemical potential of species k
z_k	valence of species k
$c_k(x)$	free concentration of ionic species k
$C_k(x)$	total concentration of ionic species k
$S(x)$	position-dependent concentration of structural net charge
$V(x)$	electric (Coulombic) potential
$\epsilon(x)$	position-dependent relative permittivity
ϵ_0	permittivity of the vacuum
e_0	elementary charge
k_B	Boltzmann constant
T	absolute temperature
N_A	Avogadro's number
I	mean net current across open pore
γ	mean slope conductance of open pore
V_m	transmembrane voltage, inside versus outside

Note that the excess chemical potentials, μ^0, describe all interactions between an ion and its pore environment that are not captured by PNP0 theory. PNP0 is concerned with ideal electrolyte solutions and the mean electric field that results when volume elements of these solutions contain a net ionic charge. Excess chemical potentials are often expressed as activity coefficients.

The one-dimensional formulation of PNP2 disregards gradients in the nonaxial dimensions of the domain (Romano and Price, 1996). It is exact for a domain of uniform cylindrical, conical, or (hemi)spherical shape, whose lateral boundaries confine the ionic flux and the electric field. The actual domain (Fig. 1) includes a central, cylindrical pore (typically 1 nm long, with a 0.3-nm radius) flanked on each end by a 2-nm-long conical atrium that opens with an aperture angle of 45° into a hemispherical subdomain of the bulk solution (10-nm radius). In solving the PNP2 equations numerically, this complex geometry is approximated by a conical stack of segments whose aperture angle varies with position in the pore axis, and the grid resolution for numerical integration is varied in proportion to the surface area of the cone faces. The portion of the electric field that extends from the pore lumen into the channel protein and membrane lipid is neglected, because computations using an analysis given by Barcilon (1992) showed that this simplification has very small effects in the presented model.

Because of the chemical affinities assigned to ions in Eq. 1, ions will partition in a species- and position-dependent manner between the far bulk and the pore. This partitioning

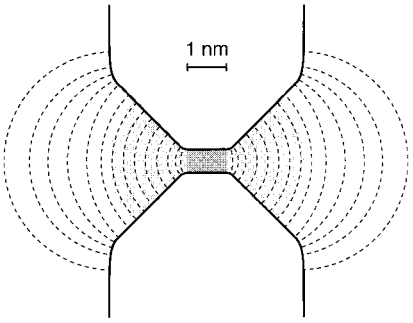

FIGURE 1 Geometry of the pore and the integration domain. The sketch shows an axial cross section through the model Ca channel pore. Solid lines mark the pore walls. The dark-shaded zone indicates the cylindrical pore proper, where structural charges are located and excess chemical potentials and diffusion coefficients differ from those in bulk solution. This pore section is 1 nm in length and 0.6 nm in diameter (McCleskey and Almers, 1985). The dashed lines indicate some of the equipotential (and equiconcentration) surfaces used in the one-dimensional approximation of pore geometry. These surfaces were chosen to be perpendicular to the atrial channel walls, as necessary if the electric field is confined to the aqueous lumen of the pore. The actual integration domain was larger than the outermost surface shown: it extended 10 nm into each bulk solution. In subsequent graphs (Fig. 4), the central pore segment (*dark gray*) will be represented on a 1:1 scale, with the atrial (*light gray*) and bulk domains (*white*) of the integration domain represented in compressed scales (1:2 and 1:100, respectively); the x-coordinate in these plots corresponds to the pore axis.

is not saturable per se, but is limited by Coulombic repulsion. Ions have the freedom to move according to their specific (and position-dependent) diffusion coefficients. The Na, Ca, and Cl ions considered in this analysis behave in this fashion. Thus their total and free concentrations are identical.

The analysis also includes protons. Unlike the other ion species, protons are allowed to combine stoichiometrically with some of the structural charge (e.g., unprotonated glutamate carboxyl groups). This form of binding is saturable; the bound protons are immobile, and do not contribute to the proton flux. Therefore, the total concentration of protons in the pore (C_H) is generally different from their free concentration in the pore (c_H). The titration of structural charged groups is described as a reaction in equilibrium because PNP2 theory is concerned with the temporal average of flux and, hence, temporally constant ionic concentrations. If there is only one kind of titratable structural charge, the total proton concentration in the pore is related to the free proton concentration in the pore by

$$C_H(x) = c_H(x)\left(1 + \frac{(1-f)S(x)}{k_D + c_H(x)}\right) \tag{4}$$

where the new symbols are f, the fraction of the structural charge (S) that cannot be protonated, and k_D, the (local) dissociation constant of the structural charge.

The dissociation constant, k_D, applies to glutamate residues and protons as observed in the local environment of the pore. k_D is generally different from an apparent dissociation

constant, which relates the degree of dissociation to the proton concentration in the bulk solution and which includes, for instance, the effects of the local electric potential in the pore on the local concentration of protons.

In the Ca channel model, excess chemical potentials and diffusion coefficients of ions are treated as generally dependent on position, but as invariant otherwise, e.g., with respect to ion concentrations. This assumption is preliminary and will have to be reconsidered in future improvements of the model. For instance, ionic activities and mobilities vary substantially with concentration, even in bulk solutions, at concentrations lower than those considered for the pore (Robinson and Stokes, 1959, Appendices 6.3 and 8.1). On the other hand, if the mobile ions in the pore maintain a relatively constant total concentration (as required for neutralization of the structural charge), concentration-dependent ionic parameters would be buffered even when bulk concentrations are varied. This subject is considered further in the Discussion.

DETERMINATION OF MODEL PARAMETERS

When the electric field and ionic concentrations are constant in space, the Nernst-Planck equation (Eq. 1) implies that the conductivity of the electrolyte in the pore is given by

$$\kappa = \frac{e_0^2 N_A}{k_B T} \sum_k z_k^2 D_k c_k \tag{5}$$

A measurement of this conductivity, under conditions where one ion species is dominant and its concentration is known, immediately yields the diffusion coefficient of the species. Once the diffusion coefficients are known, further measurements of the conductivity under conditions where two species compete for the pore reveal their concentrations in the pore. From the partitioning between the bulk and the pore, we can calculate the relative electrochemical potentials of the ions in the channel's pore. Used in this way, a few measurements of pore conductance suffice to estimate the essential free parameters for a PNP2 model.

This approach implies that the diffusion coefficients and electrochemical potentials, as well as the structural charge, are uniform over the conductance-limiting segment of the pore. We therefore start with the assumption that the central, cylindrical part of the pore has uniformly distributed parameters (the atria and near bulk are assigned zero structural charge and chemical affinities, and diffusion coefficients identical to those in bulk water). Nevertheless, asymmetrical ionic conditions, boundary layers at the edges of the central pore region, and the effects of flux make concentrations and the electric field nonuniform. The actual boundary layers are computed by solving the full PNP2 equations, and the effects of boundary layers can be assessed by comparing the conductances expected for uniformity with the full computations. Because the full theory is constructed using only data obtained under symmetrical ionic conditions and with small test voltages, ionic currents computed for asymmetrical ionic conditions and large applied voltages are predictions that can be used to test the theory.

To evaluate conductivity measurements made near thermodynamic equilibrium, we use the equilibrium (zero flux) limit of the PNP2 equations, the Poisson-Boltzmann equations. We also replace Poisson's equation by the postulate of electroneutrality (as in a macroscopic Donnan system). The concentrations appearing in the conductivity equation (Eq. 5) then obey Eq. 4 and

$$\sum_k z_k C_k + S = 0 \tag{6}$$

$$c_k = c_{B,k} \exp\left[-\frac{z_k e_0 V_D + \mu_k^0}{k_B T}\right] \tag{7}$$

where the new symbols are $c_{B,k}$, bulk concentration of species k, and V_D, the Donnan potential (pore relative to bulk).

Equations 6 and 7 define the ion concentrations and electric potential in the pore uniquely if the excess chemical potentials of the ions are known. The inverse calculation does not have a unique solution: with any value selected as the electric potential, a compatible excess chemical potential can be computed from each ion's pore concentration via Eq. 7. In the following, we define the excess chemical potential for protons as zero. Using Eq. 7 for protons, we compute the electric potential, and with the electric potential known, the standard chemical potentials of the other ions follow from their Eq. 7. Thus the absolute potentials remain undetermined within an offset equal to the actual excess chemical potential for protons, but changes in electric potential associated with changes in bulk concentrations can be predicted correctly from the excess chemical potentials obtained from this analysis, as can current through the channel.

The titratable structural charge, $(1 - f)S$, and its proton dissociation constant, k_D, are treated as inputs to the theory. Concentrations of this part of the structural charge are assigned values that correspond to one to four carboxyl groups. The dissociation constant of glutamate residues in an aqueous environment, corresponding to a pK_A of 4.6, is used to describe protonation of this structural charge (Creighton, 1984). This leaves the nontitratable charge, fS, ionic diffusion coefficients, and the excess chemical potentials of all ions except protons as free parameters.

These parameters are estimated from conductance measurements by assuming that both the Cl ion concentration in the pore and proton flux are negligible, reducing the number of relevant free parameters to five (f, D_{Na}, D_{Ca}, μ_{Na}^0, and μ_{Ca}^0). These free parameters can be analytically determined by applying Eqs. 4–7, using the following values approximated from experimental measurements on L-type Ca channels.

1. The Na-supported pore conductance in a Ca-free NaCl solution at pH $\geq$ 9 (where proton block does not occur) is $\sim$100 pS (Hess et al., 1986, report 85 pS under similar ionic conditions).

2. Lowering the pH from 9 to 6 blocks maximally 75% of the (Na) conductance measured in experiment 1 (Pietrobon et al., 1989).

3. Lowering the pH from 9 to 7.5 blocks about one-half of the pH-sensitive fraction of the (Na) conductance measured in experiment 1 (Pietrobon et al., 1989).

4. The addition of 1 μM Ca ion to a Ca-free NaCl solution at pH 7.5 reduces the conductance to about one-half of that measured at $<10^{-8}$ M Ca (Almers et al., 1984; Hess and Tsien, 1984).

5. The maximum Ca-supported pore conductance in saturating Ca solutions is ~10 pS (Hess et al., 1986).

Note that Eqs. 4–7 describe an ion exchange resin (i.e., a channel) bathed in a uniform solution, whereas the experimental measurements were typically obtained with asymmetrical Ca and proton concentrations.

In experiment 1, Na is the only significant charge carrier in the pore. Because of electroneutrality, the pore concentration of Na is close to the concentration of negative structural charge. Equation 5 then yields an estimate of the diffusion coefficient for Na. Experiment 5 is used to estimate the diffusion coefficient for Ca by the same method.

pH 6 in experiment 2 is low enough to saturate the structural groups that can be protonated with an apparent pK_A of 7.5 (experiment 3). Neutralization of structural charge leads to a reduction of Na concentration in the pore, as indicated by the percentage reduction of (Na supported) pore conductance. Hence this experiment yields a direct estimate of the fraction of the structural charge that can be protonated in the pH range 6–9. We assume that the charge that can be protonated arises from the carboxyl groups of glutamate residues, and interpret the apparent shift of pK_A (from 4.6 to 7.5) as a consequence of a negative potential that attracts protons from the bath into the pore. The fraction of structural charge that cannot be protonated is not specified and is treated as a free parameter. Experiment 2 indicates that 0.75 of the total structural charge can be protonated. Hence, if we assume that the channel has two glutamate residues, the total charge (glutamates plus nonprotonated charge) must be equivalent to $2/0.75 = 2.67$ elementary charges.

Experiments 3 and 4 assess the proton or Ca concentrations needed to displace about one-half of the Na concentration from the pore. These data yield estimates of the excess chemical potentials for Na and Ca ion (relative to that for protons, which is taken as zero).

The results of this approximate algebraic analysis are summarized in Table 1. The analysis was repeated with four different structural charge concentrations, involving one to four carboxyl groups in the cylindrical pore of Fig. 1 (one elementary charge per pore is equivalent to ~6/0.75 M of monovalent ions). The algebraic analysis was verified by solving the complete equations 4–7 numerically with the estimated pore parameters.

Fig. 2 plots the computed pH and Ca dependences of pore conductance (Fig. 2 *A*) and the computed electric Donnan potential (Fig. 2 *B*) versus the bath concentration of the test ion; the graphs shown apply to a structural charge comprising four carboxyls per pore volume. Fig. 2 *A* confirms that the conductance in NaCl solution (with 10^{-12} M Ca ion) approaches 100 pS at high pH and decreases with an apparent pK_A close to 7.5 as pH is lowered (*dashed curve*). The conductance levels off near pH 6 (and actually shows a secondary increase due to a proton conductivity at pH < 4). At pH 7.5, about one-half of the proton-sensitive conductance is available (*left end of the solid curve*), and the addition of Ca ion to the bath reduces the conductance to the level supported by Ca conduction, 10 pS. Reduction to one-half of the Na conduction level is reached near 1 μM Ca ion. Note that this behavior of the conductance does not involve an anomalous mole fraction effect, like that experimentally found for the current through Ca channels (Almers and McCleskey, 1984; Hess and Tsien, 1984). The latter effect is reproduced by the PNP2 model, as will be shown below.

The electric potential corresponding to the situation of experiment 4 is of particular interest. Here, 1 μM Ca ion applied in the bulk solution is equipotent with ~100 mM Na ion in competing for the pore. The affinity for Ca, as expressed by the apparent binding constant, is $\sim 10^5$ times larger than that for Na. The electric potential V_D (pore resin relative to the bulk solution) of ~ −150 mV at 1 μM Ca (Fig. 2 *B*, *solid curve*) is one factor that favors the entry of Ca over that of Na, by a factor of ~300 (corresponding to an affinity difference of 150 meV). This is about the square root of 10^5. In terms of binding free energy, about one-half of the Ca/Na affinity difference is explained by Coulombic interaction with structural charge. The structural charge

TABLE 1 Parameters for the PNP model

Carboxyls	f	S (M)	D_{Na} (10^{-12} m^2/s)	D_{Ca} (10^{-12} m^2/s)	μ^0_{Na} (10^{-3} eV)	μ^0_{Ca} (10^{-3} eV)
1	0.25	7.83	12	0.601	76.1	−76.3
2	0.25	15.66	6.01	0.301	58.3	−94.1
3	0.25	23.49	4.01	0.200	47.9	−104.5
4	0.25	31.32	3.02	0.150	40.5	−111.9

Four structural charge densities (S), including to one to four carboxyl groups per pore (local pK_A 4.6) and a fraction (f) of nonprotonizable charge, were used in the computation of diffusion coefficients (D) and excess chemical potentials ($\mu°$) for Na and Ca ions. Nonessential parameters (not defined by the data) were the diffusion coefficient for protons (set to be seven times that computed for Na ion), and the diffusion coefficient of Cl (chosen to be equal to that computed for Na); the affinity for protons was taken as 0, and the affinity for Cl ion was made equal to that computed for Na ion. The relative permittivity of the pore proper, atria, and bulk solutions typically was set to 80 (except in Fig. 6 *D*, where the permittivity of the pore proper was varied). Note that excess chemical potentials are given as the change in Gibbs' free energy for moving one ion from the bath to the pore.

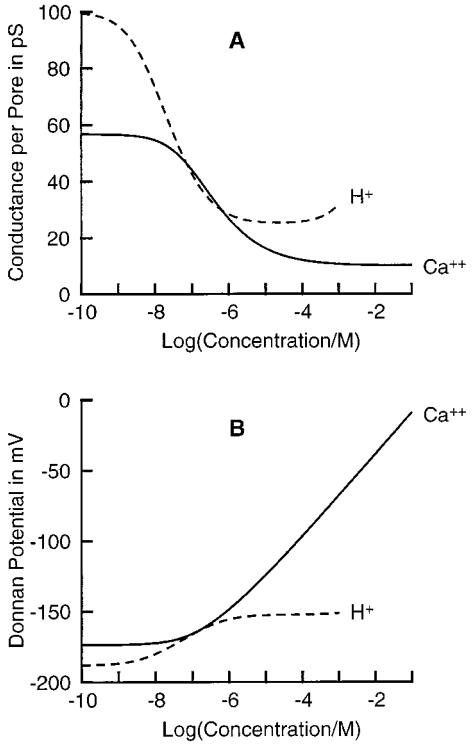

FIGURE 2 Conductivity (*A*) and Donnan potential (*B*) as computed for the hypothetical "resin" of the Ca channel. The conductivity is expressed in terms of the equivalent single-channel conductance (for the dimensions of the cylindrical pore in Fig. 1). The Donnan potential corresponds to the voltage expected between the pore and the bath. Dashed curves give the conductivities and potentials computed for increasing concentrations of HCl added to the bath, which contains 10^{-12} M $CaCl_2$ and 150 mM NaCl. For solid curves $CaCl_2$ is added to the bath, which contains 150 mM NaCl (pH 7.5). The abscissa plots the concentration of the salt being added. Curves were computed by solving Eqs. 4–7 with the parameters listed in Table 1; the fixed charge of the resin was chosen to include four carboxyl groups per pore.

cannot generate a more negative electric potential in the pore (and hence contribute more to this selectivity), because at −150 mV the proton concentration in the pore corresponds to a pH 2.5 units below that in the bulk solution, enough to protonate a significant fraction of glutamate carboxyl groups whose pK_A is ~4.6.

Table 1 reveals relationships between model parameters and the number of carboxyl groups assigned to the pore. The diffusion coefficients scale inversely with that number, which essentially limits the concentration of charge carrier in the pore. The Na:Ca ratio of the diffusion coefficients is 20, as expected from the Na:Ca conductivity ratio and the valences. The differences between the excess chemical potentials for Na and Ca are invariant, but the individual chemical potentials vary by 18 meV for each twofold variation in the number of carboxyls. Graphs of the electric potential in the resin were identical for all numbers of carboxyl groups; the computed conductances were also superimposible, except for small variations due to the proton conductance predicted for low pH. Thus the experimental information used to construct the pore resin was equally well reproduced with all considered choices for the number of carboxyl groups. This degeneracy was largely preserved when the resin was included in the PNP2 model (see below).

The model parameters are nonunique for another reason already mentioned: the absolute excess chemical potentials are undetermined within an offset (the proton chemical potential; see above). A different k_D of the structural charged groups would have effects indistinguishable from those resulting from a different chemical affinity between protons and the pore (in the absence of a measurable proton current). Negative Coulombic potentials of the proposed magnitude are plausible, as they can account for much of the selectivity between mono- and divalent cations, as well as for the selectivity against anions. Even with Ca concentration approaching 100 mM, the pore maintains a negative potential unfavorable to the entry of anions (Fig. 2 *B*, *solid curve*).

The source code (in C) of a library of PNP2 functions is available for anonymous ftp at ftp.rush.edu in /pub/Eisenberg/Nonner.

RESULTS

Using the model parameters estimated by analysis of a hypothetical pore resin, the PNP2 equations (Eqs. 1–4) were integrated numerically to predict the behavior of the pore under applied potentials and/or concentration gradients. Such computations constitute predictions, because the parameters were estimated for near-equilibrium conditions with the resin surrounded by a uniform solution. The following simulations do not involve any further model optimizations or changes in any parameters, except where the effects of parameters were studied by variation.

Fig. 3 *A* plots current/voltage (*I*/*V*) relationships predicted for a model Ca channel lined with four carboxyl residues at different bath Ca (10^{-9} to 10^{-1} M). The channel was bathed in symmetrical 150 mM NaCl, with $CaCl_2$ asymmetrically added to the external solution. A pH of 9 was maintained on both sides to minimize protonation of structural charge (this virtually eliminates proton block, which is considered below). Fig. 3 *B* replots the *I*/*V* curves for the three largest Ca concentrations with an expanded current scale. These theoretical *I*/*V* curves reproduce the following properties of L-type Ca channel currents:

1. The currents are large and vary linearly with voltage when external Ca concentrations are $\leq 10^{-7}$ M. These currents are carried by Na ion, and their sign reverses at 0 mV because of the symmetrical Na concentrations. Single-channel currents from Ca channels bathed in salines containing Ca chelator and alkali cations have these features (e.g., figure 11 of Hess et al., 1986).

2. External Ca concentrations greater than or equal to 10^{-3} M yield smaller currents. Here, inward currents carried by Ca increase almost linearly with voltage. Outward currents carried by Na vary hyperbolically. The slope of the *I*/*V* curves is minimal around their reversal potential. The

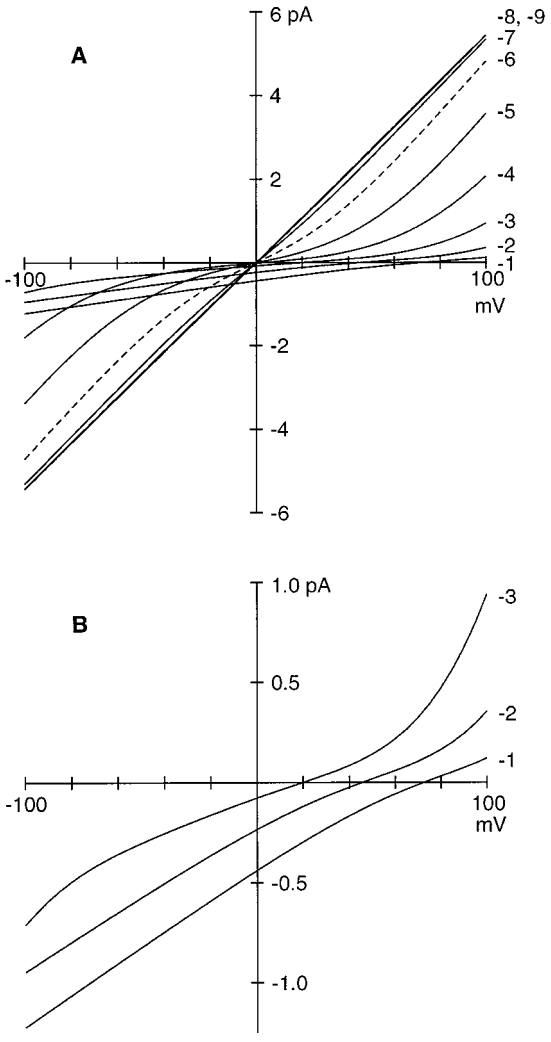

FIGURE 3 Theoretical current/voltage curves at various extracellular Ca concentrations. The solutions contained symmetrical 150 mM NaCl. $CaCl_2$ was added to only the extracellular solution in 10-fold increments from 10^{-9} to 10^{-1} M (the curves are labeled with the exponent of the power of 10, e.g., -9 for 10^{-9}). The pH was 9 on both sides. (*A*) Plots of the entire set. (*B*) The three *I/V* curves computed for 10^{-3} to 10^{-1} M with an expanded current scale. The model parameters are given in Table 1 (four carboxyl groups).

reversal potential increases by 25 or 29 mV when external Ca concentration is increased from 1 to 10 mM, or from 10 to 100 mM, respectively. Experimental *I/V* curves obtained under similar ionic conditions, or with Ba as the divalent ion, have these features (e.g., figure 8 of Lee and Tsien, 1983; figures 8–10 of Hess et al., 1986).

3. Currents computed for an external Ca of 10^{-6} to 10^{-4} M have complex characteristics. With increasing voltages these *I/V* curves bend hyperbolically toward the linear relationship measured in the virtual absence of Ca. At potentials between 0 and -35 mV, such currents are smaller than both of the currents carried in the absence of Ca or in the presence of 10 mM Ca. This is the anomalous mole fraction effect (AMFE) of the current in Ca channels (Almers and McCleskey, 1984; Hess and Tsien, 1984). This AMFE is considered in more detail below.

Fig. 4 plots some of the transpore profiles of the electric potential and of the Na, Ca, and Cl concentrations that underlie the *I/V* relationships of Fig. 3; panels *A–D* and *E–H* refer to transmembrane voltages of 0 and -100 mV, respectively. The subsections of the domain in which the PNP2 equations were solved (Fig. 1) are represented by shades of gray, using different degrees of abscissa compression to focus on the cylindrical pore (*dark gray zone*) and the atria (*light gray zones*). Each curve applies to one external Ca concentration, which was varied in steps of 10-fold between 10^{-9} and 10^{-1} M as in Fig. 3.

In Fig. 4 *A* the electric potential is distributed almost symmetrically at the lowest Ca concentration and becomes asymmetrical as the external Ca concentration is increased. Like the Donnan potential plotted in Fig. 2 *B*, the potential in the microscopic pore reaches ~ -170 mV for the lowest Ca concentration and increases toward zero as the Ca concentration is increased. The Coulombic potential change reflects the exchange between Na and Ca in the pore, and its range is equivalent to the difference in the standard chemical potentials of the two ions, ~150 meV (Table 1). Thus, as Ca (which is chemically attracted) is replaced with Na (which is chemically repelled), a negative Coulombic potential builds up that compensates for the change in chemical interaction. The pore keeps its net charge closely balanced, because a relatively small cation deficit suffices to create the negative Coulombic potential.

The transition toward the bulk potential in Fig. 4 *A* begins ~0.2 nm away from the ends of the cylindrical pore section (1 nm in length), but mostly occurs in the narrow parts of the atria. Thus the central part of the pore, where the negative structural charge is located, maintains its own potential up to near its edges. This potential attracts cations, both Na and Ca, as shown in Fig. 4, *B* and *C*. In addition, the concentrations of these ions undergo jumps at the cylinder/atrium boundaries, because the standard chemical potentials of the ions are discontinuous. Ca ion is attracted to the pore by a chemical affinity, whereas Na is repelled (see Table 1). As a consequence, Ca concentrations are rather uniform and high throughout the pore, but Na concentrations tend to be low near the edges of the pore. The deficit in cations in the outer cylindrical regions is compensated for by a particularly high Na concentration in the adjacent zones of the atria. Apart from these localized deviations from electroneutrality, the concentrations of Na and Ca together are equivalent to the concentration of structural charge, ~31 M (Table 1). When external $CaCl_2$ is added, Ca is exchanged for Na: the electrostatic sites provided by the negative structural charge are always occupied by cations. It is also interesting to note that the preferred locations of the two ion species are not identical: Ca ions always concentrate inside the pore proper, whereas Na ions also tend to dwell just outside the pore proper.

In the PNP2 model, the diffusion constants of Na and Ca are small only in the pore, and jump to their bulk values at

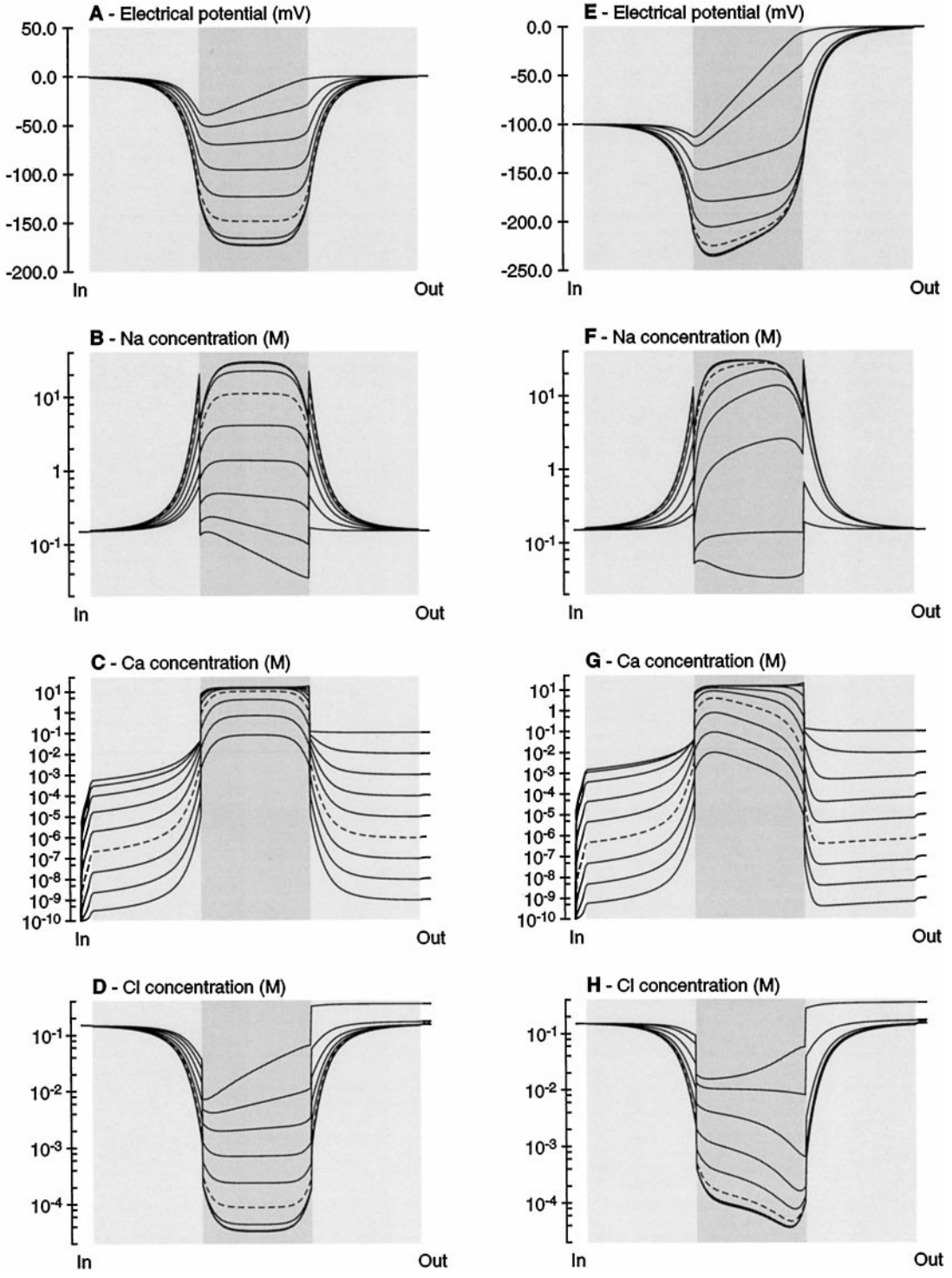

FIGURE 4 Profiles of electric potential and Na, Ca, and Cl ion concentrations as a function of bulk extracellular [Ca]. These profiles correspond to the *I/V* relationships plotted in Fig. 3. Two transmembrane potentials are represented: 0 mV (*A–D*) and −100 mV (*E–H*). The abscissa is nonlinear; the bulk section (*white background*) and atrial sections (*light gray*) are compressed 100- or 2-fold compared to the pore proper (*darker gray*). The actual dimensions are given in Fig. 1. The solutions contained 150 mM NaCl (pH 9); $CaCl_2$ was added to the extracellular solution in 10-fold increments from 10^{-9} to 10^{-1} M (the curves corresponding to 1 μM Ca are shown as *dashed lines*).

the cylinder/atrium boundaries. Thus if a pore is to have high conductance, like a real Ca channel, the charge-carrying cations must have high concentrations throughout the pore. This is largely the case for Ca ions, whereas Na ions have a zone of relative depletion near the edges of the pore. The effect of this boundary layer is to reduce Na conductance more than Ca conductance with respect to the ideal condition, in which concentrations are constant and high

throughout. This is reflected in the amplitudes of the Na and Ca currents in Fig. 3. Although the Na diffusion constant of the pore resin was selected to give a Na conductance of 100 pS at high pH and low bath Ca, the plotted current amplitudes yield a conductance less than 60 pS. The maximum Ca conductance is ~8 pS, close to the targeted value of 10 pS. The microscopic dimensions of the pore do not dramatically alter the projections from the macroscopic analysis, because the high concentration of structural charge attracts counterions in high ionic strength, which screen the structural charge within a short Debye length. Thus boundary regions are significantly shorter than the pore length.

Cl ion concentrations in the pore (Fig. 4 *D*) increased with increasing Ca concentration (because the electric potential in the pore became less negative; Fig. 4 *A*) and approached the Na concentration when Ca concentration reached 0.1 M. Because of their low concentration in the pore, Cl ions did not contribute a significant flux. This also applies to protons. With 10^{-9} M protons in the bulk solutions, the proton concentration in the pore reached 10^{-6} M in the absence of Ca and was reduced to less than 10^{-8} M when external Ca approached 0.1 M. Over the same range, the protonated fraction of structural charge dropped from ~1 M (out of 31 M) to less than 10^{-2} M. Computed effects of higher bulk concentrations of protons on Na and Ca currents are described in a later section.

Atrial diffusion polarization

The PNP2 equations were integrated over a domain that includes atria and 10 nm of bulk solution on each side (Fig. 1). We therefore can assess the diffusion polarization that occurs in these access paths that might reduce the currents supported by the pore. Fig. 4, *E–H*, plots transpore profiles that are analogous to those of Fig. 4, *A–D*, but which are calculated with a strong applied voltage, −100 mV. This gradient drives strong inward fluxes of both Na and Ca (*from right to left* in the profiles). The electric potential (Fig. 4 *E*) is almost linear in the pore (as would be expected from Ohm's law for a region of uniform resistance) and approaches the far-bulk potentials within the length of the atria. The largest Na currents flow when external Ca is very low; the Na concentrations in the atria then are higher than those in the bulk and almost symmetrical (Fig. 4 *F*). In contrast, Ca currents, which flow when external Ca concentration is raised, cause the external atrial Ca concentration to become lower (up to twofold) than the external bulk concentration (Fig. 4 *G*). This decrease in concentration in the outer atrium is accompanied by an increase in concentration in the inner atrium. At Ca concentrations below 10 mM, this polarization of atrial concentrations becomes significant: Ca concentrations in the pore proper are lower on the outer than on the inner side. Thus Ca fluxes at submillimolar external Ca are limited by diffusion polarization in the access path to the pore, as can be seen from the linear relationship between Ca flux and external Ca concentration (Fig. 7). Although the pore geometry used in the model is a crude estimate and the one-dimensional approximation is not exact (Romano and Price, 1996), these calculations show that an accurate assessment of Ca fluxes must consider the geometry and structural charges of atrial regions.

The anomalous mole fraction effect

Fig. 5 *A* plots the magnitude of inward currents computed for a transmembrane voltage of −10 mV versus the concentration of external $CaCl_2$ (symmetrical 150 mM NaCl, as in Fig. 3). The theory predicts a minimal current near 10^{-4} M. Both the Na currents at very low Ca concentrations and the Ca currents at millimolar Ca concentrations are larger. The model thus reproduces the anomalous mole fraction effect of the current in the Ca channel described by Almers and McCleskey (1984) and Hess and Tsien (1984). This may appear unexpected, because the hypothesized pore resin does not reveal a comparable minimum of conductivity (Fig. 2 *A*). The experimental AMFE, however, is based on a measurement of current performed at a fixed voltage. Because with the unilateral increase in external Ca the reversal potential for the total current shifts from zero to positive voltages (cf. Fig. 3 *B*), the increase in the current at millimolar Ca concentrations largely reflects an increase in

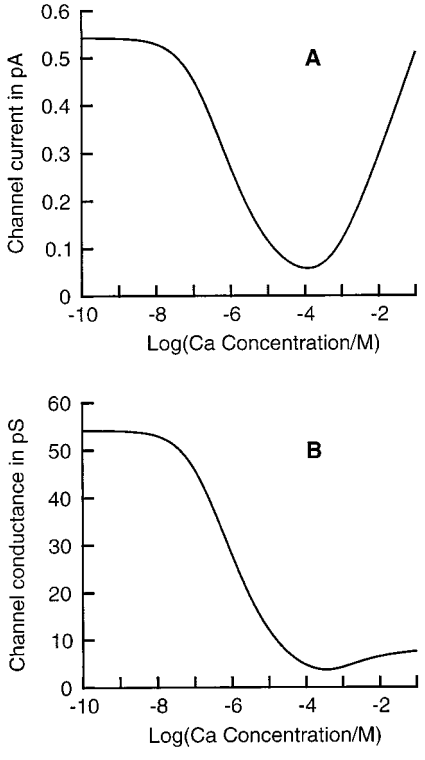

FIGURE 5 Anomalous mole fraction effects. (*A*) Theoretical currents (at −10 mV applied potential) versus external Ca concentration. (*B*) Theoretical slope conductances under the same conditions as in *A* for a 5-mV interval centered about −10 mV. Both internal and external solutions contained 150 mM NaCl, pH 9. Model parameters are given in Table 1 (four carboxyl groups).

effective driving force rather than an increase in conductance. The corresponding simulated conductance (Fig. 5 *B*) exhibits a much smaller increase at millimolar Ca than the simulated current. The shallow minimum in this conductance results from an ionic-strength effect: as Ca ion concentration is increased, the Ca concentration in the boundary layers of the pore (Fig. 4 *C*) is increased slightly. Because the Ca diffusion coefficient is small there, this has an appreciable effect on overall conductance.

The finding that simulations based on the PNP2 model can predict the AMFE suggest that in the L-type Ca channel the actual AMFE of conductance is much smaller than the AMFE of current described in the classical publications (Almers and McCleskey, 1984; Hess and Tsien, 1984). Because ionic strength was also varied, these experiments do not use the stringent conditions normally applied to experimental assessments of AMFEs (Eisenman et al., 1986). The AMFE of monovalent ion channels (like the mixed alkali effect of electrochemistry; Wilmer et al., 1994) is defined as a property of conductances, not current, measured in symmetrical solutions whose contents are varied at constant ionic strength.

The current-AMFE observed in Ca channels has been interpreted to require a pore that accepts more than one ion and forces ions to move in single file (Almers and McCleskey, 1984; Hess and Tsien, 1984). In contrast, the PNP2 model describes the average locations of ions and does not impose any logistic constraints on the movements of individual ions. Fig. 6 *A* shows the current-AMFE as predicted for different concentrations of structural charge corresponding to one to four carboxyl residues per pore. Fig. 6 *B* plots the computed numbers of Na and Ca ions present in the pore. The current-AMFE is expressed in all cases, even when the structural charge includes only one carboxyl group and the pore proper holds on average less than one Na or Ca ion. Thus the presence of four carboxyl groups in the actual Ca channel is not what produces the current-AMFE, just as multiple (mean) occupancy is not required for the conductance AMFE (Nonner et al., 1998). This result contrasts with the previous models that require multiple occupancy to produce a current-AMFE. Mean-field theories like PNP2 compute electrostatic screening effects, which are present at any ionic strength, whereas these effects cannot be captured in theories that treat electrical interactions in the way of repulsion factors among discrete bound ions (Hille and Schwarz, 1978).

The amount of structural charge affects Na currents through the model channel more than Ca currents (Fig. 6 *A*). Reducing the structural charge reduces the ionic strength in the pore (Fig. 6 *B*) and hence increases the width of the boundary layers at the pore entrances. This effect is stronger with monovalent than with divalent cations, and thus creates wider zones of relative depletion for Na than for Ca. In effect, the channel with the lower structural charge does not conduct Na as well as that with higher charge, whereas their Ca conductances are very similar. This appears paradoxical in light of the observation that Ca channel sequences conserve four glutamate residues in the proposed pore lining region (EEEE locus), whereas Na channels have two carboxylic and one basic residue conserved in these positions (DEKA locus), and it appears incompatible with the results of point mutation experiments decreasing the number of

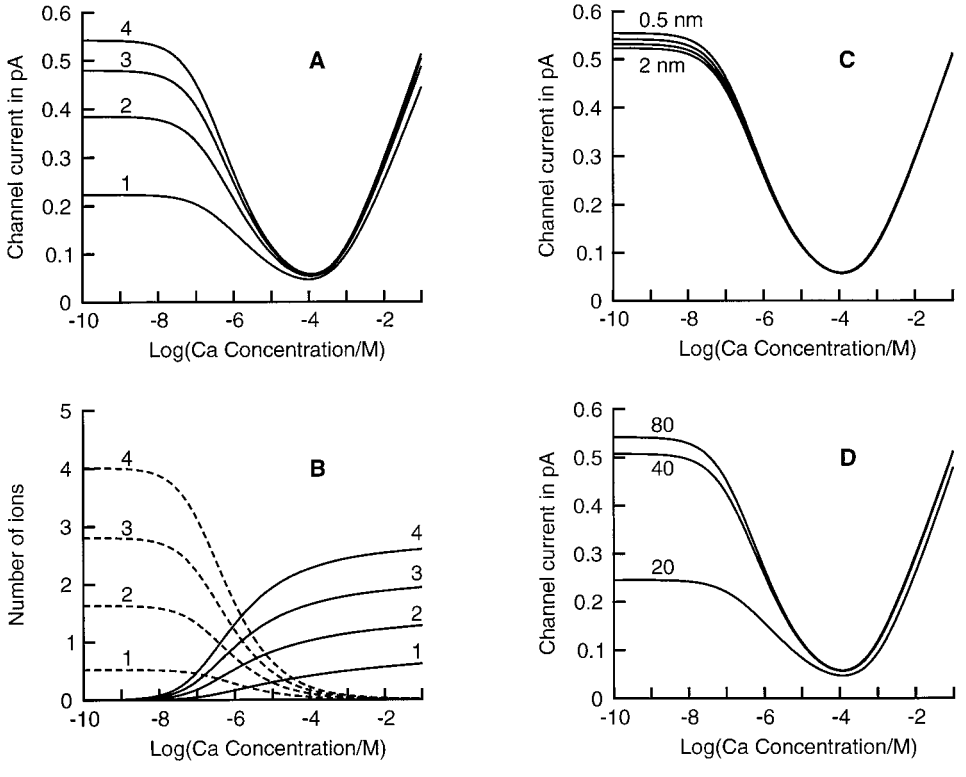

FIGURE 6 Current-AMFE with varied structural parameters. (*A*) AMFE (−10 mV) computed for model pores containing one to four carboxyl residues. Other parameters are as given in Table 1. (*B*) Average number of Na and Ca ions present in the pore proper under the conditions of *A*. – – –, Na ion. ——, Ca ion. (*C*) AMFE computed for various lengths of the pore proper: 0.5, 1, 1.5, and 2 nm. Diffusion coefficients were adjusted in proportion to pore length with respect to the standard values shown in Table 1. (*D*) AMFE computed for various relative permittivities in the pore proper: 20, 40, and 80. Four carboxyl groups.

glutamate residues (Yang et al., 1993; Ellinor et al., 1995), which lead to a reduction of Ca affinity with respect to monovalent cations.

We did not attempt to mimic the actual effects of differently composed charge clusters or point mutations, because to do so at this stage would have required ad hoc assumptions about variations in excess chemical potentials. We suggest for the time being that the cluster of four glutamate residues has a role beyond generating Coulombic force. These residues might actually create the excess chemical potentials that we only describe in this paper. The computational result that only a fraction of the putative structural charge of a Ca channel is needed to generate the observed conduction characteristics also suggests that the high density of structural charge has a significance that is not made explicit by the present model. An electrochemical theory of excess chemical potentials, adapted to the geometry of ionic pores, will be needed to interpret these aspects of the EEEE cluster (see Discussion).

The effects of channel length are surprisingly small. Fig. 6 *C* plots the AMFE computed with four carboxyl groups, with the pore length varied between 0.5 and 2 nm; diffusion constants were varied in proportion to pore length to maintain conductance. The model pore behaves, more or less, like a macroscopic system, in which boundary layers are relatively unimportant. Structural charge is diluted in a long pore, leading to an increase in boundary layer widths at the pore edges. This should reduce currents as described above, but the larger diffusion coefficients compensate for the larger width of the boundary layers.

Fig. 6 *D* plots the AMFE of current predicted for different values of the relative permittivity in the pore. Reducing permittivity from 80 to 40 and 20 reduced Na current more than Ca current, but the overall pattern was preserved. Thus the current-AMFE of the model channel is also insensitive to the dielectric properties of the pore.

An important argument made for multiple ionic occupancy of Ca channels was based on the apparent discrepancy between the high binding affinity for Ca and the large Ca fluxes supported by the Ca channel (Almers and McCleskey, 1984). With a diffusion-limited access rate and a dissociation constant of 0.7 μM, the exit rate for Ca was estimated to be $\sim$700/s, much smaller than the possible rates of Ca flux, some 10^6. Our computations show that high affinity and large flux can arise from electrodiffusion. Here, on and off rates are so strongly coupled by the electrostatic interactions quantified in Poisson's equation that they can never be considered as independent. Fig. 7 plots Ca flux versus the external Ca concentration. The flux for 1 μM Ca is $\sim$800/s, similar to the rates estimated by Almers and McCleskey and those directly observed for Ca block and unblock of unitary Li current by Lansman et al. (1986). The Ca flux of the model increases linearly over many orders of magnitude of Ca concentration, and then saturates at a level that corresponds to the observed magnitude of Ca currents.

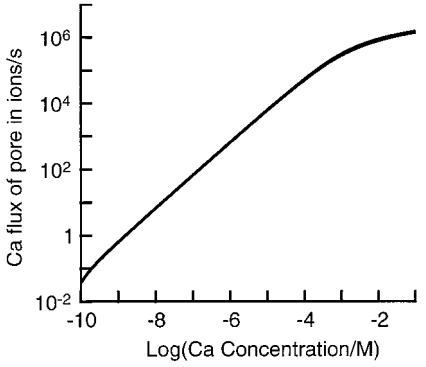

FIGURE 7 Theoretical Ca fluxes as a function of external Ca concentration. Fluxes were computed at -100 mV applied potential for one to four carboxyl groups (curves are superimposed). Other parameters are as in Table 1. $CaCl_2$ was added unilaterally to the external solution. Symmetrical 150 mM NaCl, pH 9.

Fig. 7 superimposes curves computed for different structural charges ranging from one to four carboxyl groups. The approximate electroneutrality maintained in the pore implies that the cations present in the pore are approximately equivalent to the structural charge. The near-overlap of the curves in Fig. 7 thus indicates that the number of cations in the pore is not critical for achieving appropriate Ca fluxes. This contradicts the commonly accepted notion that several Ca ions must occupy the pore to pass Ca at high rates. This test also shows that no other specific ion-ion interaction (such as Na-Ca) is needed to explain the high-conductance and high-affinity properties of Ca channels.

Appropriate Ca fluxes thus can be predicted using PNP2 theory. Appropriate Ca fluxes cannot be predicted by barrier-and-well models based on rate theory (see Appendix). In these models, charge interactions within the pore are accounted for by ad hoc interionic repulsion factors (Almers and McCleskey, 1984; Hess and Tsien, 1984), or are assumed to be negligible (Dang and McCleskey, 1998). Historically, repulsion factors have been introduced as modulating the affinities of ions that are simultaneously bound to different sites in the pore (Hille and Schwarz, 1978). There is no physical necessity for this second ad hoc assumption: ions in a pore will electrostatically interact with one another, regardless of their interactions with the pore wall. The PNP2 model does not make these ad hoc assumptions: the electric field in the pore, and the resulting interionic and ion-pore interactions, are computed by solving Poisson's equation, including all charges present in and near the pore. The prediction of appropriate Ca fluxes in this paper demonstrates that ad hoc electrostatic parameters, multiple binding sites, and the additional logistic assumption that ions move in single file are all unnecessary for predicting ion flow in Ca channels. It appears, then, that the number of ions actually accepted into the pore of a Ca channel needs to be derived from information on the structural charge provided by the channel protein.

The saturation of Ca current in high Ca

Experimental Ca currents recorded at zero membrane potential exhibit saturation when external Ca concentration is raised to tens of millimoles (Hess et al., 1986; their figure 7). The apparent k_D for this saturating current was determined to be ~14 mM, a value interpreted to reflect the affinity of the channel with respect to a second Ca ion. Fig. 8 *A* plots currents computed for such conditions from the PNP2 model as a function of external Ca concentration. The result resembles a first-order saturation curve with half-saturation below 20 mM. However, this curve describes the behavior of current, not of conductance. As for the current-AMFE plots described above, the variation in the driving force for Ca ion can account for much of the change of computed current. Fig. 8 *B* demonstrates this point by plotting slope conductance instead of current. Fig. 8 *C* shows that the variations in current and conductance computed from the model are not related to a substantial increase in total ionic occupancy: the mean occupancy is roughly constant at 2.5 Ca ions over the range 1–100 mM Ca. Rather, the conductance changes correlate with a small increase in Ca ion concentration near the outer edge of the pore (Fig. 4 *C*). This increase is small compared to the total Ca content, but fills a zone of relative Ca depletion in a region of small diffusion coefficient. Thus significant conductance changes can result from small changes in occupancy localized in strategic positions (see also Nonner et al., 1998).

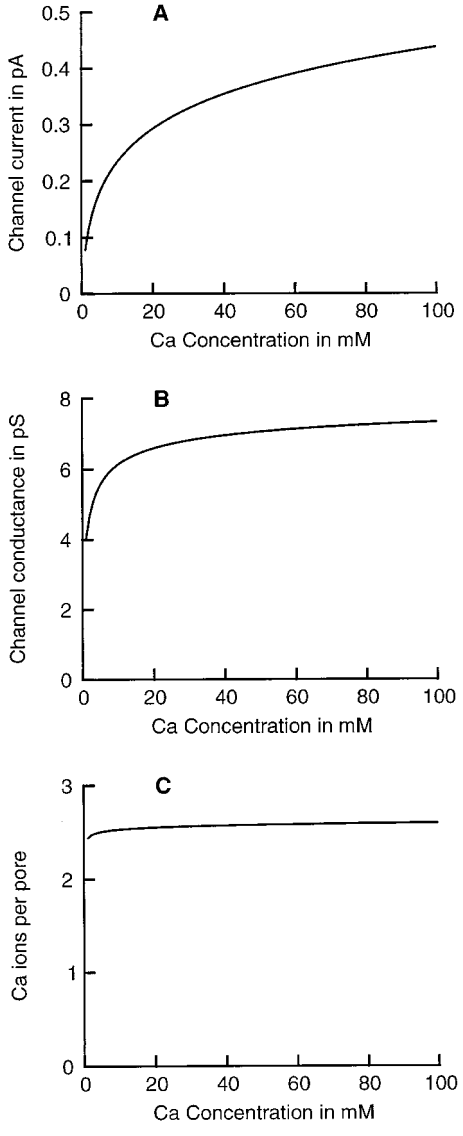

FIGURE 8 Saturation of Ca currents. (*A*) Currents computed at 0 mV versus the concentration of unilaterally applied external $CaCl_2$. These net currents are inward currents; their absolute values are shown. (*B*) Slope conductances corresponding to the currents in *A*. (*C*) Number of Ca ions present in the pore proper under the conditions of *A*. Model parameters as in Table 1 (four carboxyl groups). Symmetrical 150 mM NaCl, pH 9.

Na currents at low ionic strength

Prod'hom et al. (1989) measured the effect of lowering the ionic strength of an external Na solution on Ca channel current. They found that the Na conductance was kept almost constant for Na concentrations 20 mM or higher (their figure 4), and suggested that this buffering phenomenon arose from an external surface charge. The conductance computed for the model reproduces this kind of phenomenon (Fig. 9 *A*) without having to postulate structural charge outside the pore.

The computed number of cations (of all types) in the pore is almost constant over all tested Na concentrations (Fig. 9 *B*, *solid line*). It is interesting that there is a region where the number of Na ions decreases in exchange for protons (Fig. 9 *B*, *dashed lines*). These protons mostly bind to the carboxyl groups of the structural charge. Because flux is carried here by Na ions, and not by bound protons, the overall conductance of the pore is reduced.

This behavior shows that phenomena usually ascribed to surface charge effects can actually arise from structural charge located deep in the pore. Such electrostatic sites are highly effective in holding ions in the pore, without requiring assistance from surface charge at the ends of the channel. Fig. 9 also shows that conductance is a poor index of total ionic occupancy. Because the structural charges within the channels attract ions, the pore cannot become depleted of ions for any substantial fraction of time: it rather attracts a substitute, such as protons. Electrostatic analysis thus indicates that pore states in which one or several structural charges are not neutralized by ions (the vacant states required for ion hopping in barrier-and-well models) actually have small probabilities. Electrostatic potentials that would be created by an excess elementary charge in a channel pore have been computed by Jordan et al. (1989; their figure 3): these amount to hundreds of millivolts, equivalent to free-energy penalties of tens of kT for states with one charge vacancy. States that involve up to four such vacancies, as previously postulated to occur in Ca channels (Almers and McCleskey, 1984; Hess and Tsien, 1984), are even less

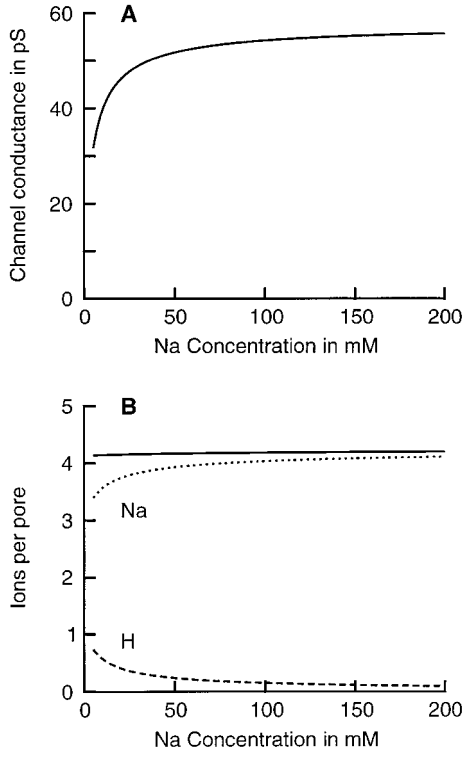

FIGURE 9 Na conductance (*A*) and channel occupancy (*B*) versus external Na concentration. The internal NaCl concentration was constant at 150 mM. Symmetrical 10^{-10} M Ca and pH 9. Model parameters as in Table 1 (four carboxyl groups). Na conductance was measured as the slope of the *I*/*V* relationship at −100 mV. Channel occupancy is the total number of ions present in the pore cylinder (*solid line*), which are mainly Na ions and protons under the chosen conditions (*dashed lines*).

likely to occur (Armstrong and Neyton, 1992). In fact, the corresponding wells in such models would have electrostatic energies severalfold higher than the barriers.

Concentration profiles computed for the lowest ionic strength used in Fig. 9 (not shown) indicate that the Na/proton exchange is relatively localized near the outer end of the pore. This creates a localized resistance whose effect on the overall conductance is relatively large compared to the percentage reduction of occupancy in the permeant species. Once again, a narrowly localized depletion layer dominates the behavior of an open channel (Nonner et al., 1998).

The pH sensitivity of Na and Ca currents

Ca channel currents carried by Na, K, or Cs are blocked by protons; the apparent pK_A value for Na current is ~7.5 (Pietrobon et al., 1989). Prod'hom et al. (1989) attributed the experimentally observed block to proton binding to an external site that interacts allosterically with the pore. Their conclusion was based mainly on a sidedness of the proton effect: when internal pH was 7.4 and external pH was varied between 6 and 9, the proton block was greater for Na influx than for Na efflux (Prod'hom et al., 1989; their figure 2). An alternative interpretation involving direct proton effects on carboxyl groups of the EEEE locus was proposed by Chen et al. (1996) on the basis of site-directed mutagenesis experiments. We used the PNP2 model to compute the extent to which these pH effects might be explained by protonation of the glutamate residues that line the pore.

The solid lines in Fig. 10 show the Na currents predicted for unilateral variation in the external proton concentration at +100 mV and −100 mV (Ca concentration 10^{-10} M). The two curves intersect. At low external proton concentration, protons accessing the pore from the intracellular side (pH 7.5) exert a block, which is enhanced at +100 mV and is weak or absent at −100 mV. When the external proton concentration is raised, the block by extracellular protons becomes dominant and is stronger for inward currents at −100 mV than for outward currents at +100 mV, the opposite of the previous situation. The apparent pK_A value for the block of inward current is higher than that for the block of outward current.

This prediction regarding the relative strengths of inward and outward current blocks agrees with the experimental findings of Prod'hom et al. (1989), but the pK_A of the simulated inward current block is nearly one unit lower than the experimental pK_A. This is not surprising, given that we designed the model to yield an apparent pK_A of 7.5 with symmetrical solutions. On the other hand, the mild proton block of outward current predicted at high external pH is not consistent with the absence of proton flicker reported by Prod'hom et al. (1989). These results suggest that a more accurate PNP2 model of proton block will have to consider nonuniformities in the properties of individual glutamate residues, which already have been proposed to underlie differential effects of point mutations (Chen et al., 1996). To this end, it will also be necessary to include time-resolved characteristics of single-proton block (Pietrobon et al., 1989; Prod'hom et al., 1989). Stochastic models of block that do not assume high barriers have been published (Bar-

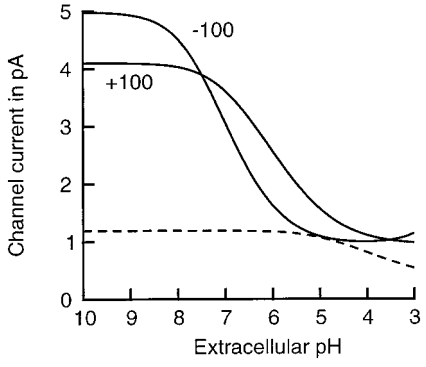

FIGURE 10 Blockade of Na and Ca currents by extracellular protons. The solid lines represent Na currents computed at +100 mV and −100 mV. Symmetrical 150 mM NaCl and 10^{-10} M $CaCl_2$; internal pH is maintained at 7.5, while the external proton concentration is varied as shown on the abscissa. The dashed line plots the absolute net current at −100 mV, computed after 10 mM $CaCl_2$ was added to the external saline. Parameters are as in Table 1 (four carboxyl groups).

kai et al., 1996), but they do not yet incorporate Poisson's equation.

Our model pore contains a 25% fraction of structural charge that is not protonated at pH 6. The degree of proton block computed for the PNP2 model actually reduces Na conductance to less than 25% (*−100 mV line* in Fig. 10). This again is an effect of lowering the ionic strength in the pore: as structural charge is protonated and Na ions retreat, the boundary layers at the edges of the pore increase in width. This creates wider depletion zones for Na and further reduces the pore conductance.

When external pH is varied in the presence of 1 or 10 mM external Ca ion, the computed Ca conductance at −100 mV is virtually unaffected in the range 9–6, but starts to decrease below pH 6 (Fig. 10, *dashed line*). The absence of block at pH 9–6 conforms with the observations of Prod'hom et al. (1989), who detected no block of Ca or Ba currents by protons.

DISCUSSION

This study applies a mean-field theory to model the average current across open L-type Ca channels. The theory uses the Nernst-Planck equation to compute ionic flux in an electrochemical gradient, and the adjoined Poisson equation to compute the electric field from the charge present in the system (Chen and Eisenberg, 1993; Eisenberg, 1996). The theory deals with the temporal averages of potential, concentration, and flux; it does not extend to fluctuations of ionic flux, such as time-resolved blockade by Ca ion or protons.

Models of ion permeation are commonly constructed and tested by fitting theoretical curves to the largest available set of experimental data; the usefulness of the model is judged by the closeness of this fit. Because theories should predict much more information than was used in their construction, we designed the PNP2 model from a subset of available observations, and then predicted observations not used in the design. We used five measurements from the literature (three limiting conductances and two crucial ion concentrations) to estimate five free parameters, and complemented this information with tentative estimates of pore dimensions (Fig. 1) and the experimentally supported hypothesis that glutamate residues line the selectivity filter of the pore. Because the parameters were estimated for conditions near thermodynamic equilibrium, all applications of the theory to nonequilibrium conditions (i.e., to conditions with significant voltage and concentration gradients) constituted predictions that can serve to test the theory. Figs. 3, 5, and 7–10 present such predictions, which show good general agreement with a wide range of published experimental results. These predictions also demonstrate that previous conclusions regarding multiion occupancy, single-file behavior, external surface charges, and allosteric proton block are not needed to explain the specific experimental observations that motivated their invention. The finding that the PNP2 model successfully accounts for multiple conduction phenomena in Ca channels suggests that some general principles of ion conduction have been captured in the theory.

One of the surprises of this and earlier work (Nonner et al., 1998) is just how little atomic detail is needed to simulate many features of channel behavior. Here, only five external parameters suffice to predict conduction and block of L-type Ca channels in the presence of Na, Ca, and hydrogen ions. All parameters are spatially uniform. Thus PNP2 makes it possible to reduce the complex conduction phenomenology of Ca channels to a few empirical constants. PNP in all its versions (i.e., Chen and Eisenberg, 1993: PNP0; Nonner et al., 1998: PNP1; this paper: PNP2) implements a self-consistent description of the electric field generated by ions and structural charges in the pore and of the diffusion of these ions under the influence of the electric field. We suggest that PNP2 models conduction efficiently because it treats electrostatics and friction appropriately.

The calculations show that Ca channel characteristics such as the anomalous mole fraction effect of Na/Ca current are quite insensitive to variation in pore length, density of lining carboxyl residues, and permittivity of the pore dielectric (Fig. 6). This robustness reflects an inherent buffering mechanism: only a small imbalance of the total concentrations of structural and ionic charges suffices to create the electric field that shapes the observed fluxes. The electrostatics of this highly charged pore also do not depend on details in the spatial architecture of groups lining the pore. Poisson's equation implies that two successive integrations over a profile of net space charge are necessary to determine the profile of electric potential, and the Nernst-Planck equation requires an additional integration of that potential profile to yield ionic flux. These integrations constitute spatial low-pass filters, and thus explain why spatial details of structural charge distribution are relatively unimportant for ion flux. In effect, the Coulombic effects of closely spaced charged residues tend to produce a single potential trough that spans the pore proper and extends into the atria of the channel, even though the structural charges are localized to the pore proper (Fig. 4 *A*).

The high affinity of the Ca channel for Ca ion has been ascribed to localized binding to one or two high-affinity sites in the pore (Almers and McCleskey, 1984; Hess and Tsien, 1984; Dang and McCleskey, 1998). In the PNP2 model, part of the Ca affinity is accounted for by the delocalized attraction into a trough of Coulombic potential, and another part is described by an attractive excess chemical potential. For Na ion, the excess chemical potential needed to fit the data is repulsive (Table 1). Thus ion selectivity in the PNP2 model of the Ca channel depends much less on specific binding than has been suggested by the previous models. Moreover, the PNP2 model accounts for a wide range of observations, although all ion-specific parameters assigned to the pore proper are given spatially uniform distributions. Spatial variations of relatively small excess chemical potentials might be expected to be unimportant for the ionic fluxes across the pore, but theoretical

computations have shown that they tend to have substantial effects when more than one permeant ion species is present (Nonner et al., 1998). Thus the absence of a spatial pattern in properties that typically involve short-range interactions is remarkable, and will have to be considered in a future theoretical analysis of the excess chemical potentials and diffusion coefficients. Such analysis indeed might be simplified if the pore proper of the Ca channel functions as one molecular ensemble, whose internal interactions are well averaged over the passage time of an ion and over the volume of the pore proper.

The significant involvement of Coulombic forces in attracting Ca to the pore has important consequences for the rates of binding and unbinding, which differ substantially from those usually expected for a high-affinity site: the rate of unbinding depends on the availability of ions that can substitute for the bound ion. The mean-field treatment of electrostatics used in PNP2 grasps this attenuation of binding force by other ions that screen the charge of a binding site from a distance, and so predicts, in particular, high Ca fluxes in the presence of physiological Ca concentrations (Fig. 7).

Our PNP2 analysis of Ca channel conduction has shown how a highly Ca-selective ionic pore can support large Ca fluxes. Large Ca fluxes have been said to involve mutual electrostatic repulsion among two Ca ions simultaneously bound in the pore (Almers and McCleskey, 1984; Hess and Tsien, 1998). Stepwise binding and unbinding of Ca have been proposed to be important as well (Dang and McCleskey, 1998). Both concepts are intrinsic to the PNP2 model described in this paper. Thus the electrostatics computed in PNP2 comprise interionic repulsion. The combination of long-range (Coulombic) and short-range binding forces results in binding energy profiles with graded transitions and relatively small jumps; furthermore, ion fluxes are limited by friction rather than by large energy barriers. The repulsion and (energy) step concepts were previously tested in Ca channel models formulated by rate theory in the tradition of Hille and Schwarz (1978); the models reproduced observed phenomena. These published models and the PNP2 model of this paper thus might appear to be alternative but equivalent physical descriptions. They are not. Rate theory as used in the published models has at least two severe inadequacies: 1) although the rate constants of the theory describe reactions in a condensed phase, they do not account for friction; 2) electrostatics are introduced into the theory by scaling rate constants with ad hoc repulsion factors. When friction equivalent to that of bulk solutions is included in these models and their electrostatics are computed by solving Poisson's equation, both the step model (Dang and McCleskey, 1998) and the repulsion model (Almers and McCleskey, 1984; Hess and Tsien, 1984) predict currents that bear no resemblance to those observed experimentally (see Appendix).

Future work will have to determine the physical basis of the excess chemical potentials described in PNP2 by ad hoc parameters. This work might be made easier because the pore of the Ca channel seems to function with a *milieu interieur* that tends to be maintained regardless of changes in exterior ionic conditions. The structural charge always attracts a closely matching number of mobile counterions because of the strength of its Coulombic field. Because of the high density of the structural charge, the mobile ions become so concentrated that their mole fractions are on the order of that of the solvent itself: the pore contains nearly as many fixed charges and ions as water molecules. In more dilute salt solutions, the dominant electrostatic interaction is between ions and solvating water dipoles. At ion concentrations as high as those in the Ca channel, the electrostatic attraction among ionic charges creates a substantial negative excess chemical potential; specific ion-ion interactions leading to ion associations would lower ionic chemical potentials even more. A repulsive potential, however, is expected to arise from the displacement of solvent volume by ions. The PNP2 model indeed uses an attractive excess chemical potential for Ca ion, but a repulsive potential for Na ion to fit the experimental currents (Table 1).

Excess chemical potentials of electrolyte solutions have long been studied in electrochemistry (where they commonly are expressed on a linear scale as ionic activity and osmotic coefficients). Recent theories, such as those based on the Mean Spherical Approximation (MSA) (Blum, 1975; Blum and Hoye, 1977; Hoye and Blum, 1978; Bernard and Blum, 1996), are capable of predicting the excess chemical potentials of ions in solutions from infinite dilution to saturation, with inclusion of specific interactions that lead to ion association. These theories consider the finite radii of ions and solvent in computing the attractive electrostatic and repulsive displaced-volume effects. They appear to be a useful basis for further analysis of the excess chemical potentials in the Ca channel. Preliminary analysis (Catacuzzeno, Nonner, and Eisenberg, with the welcome advice of Dr. Lesser Blum) shows that these theories can predict excess chemical potentials of the magnitudes listed in Table 1.

The diffusion coefficient attributed to Ca ion inside the model pore is 20 times smaller than that attributed to Na ion (Table 1); the ratio is about an order of magnitude smaller than that observed for Ca and Na ions in dilute bulk solutions. The ratio of these diffusion coefficients does not favor Ca ions: Ca selectivity instead is due to the strong electrostatic and excess chemical potentials, which both favor entry of Ca ion over entry of Na ion and override the effects of the diffusion coefficients. The absolute diffusion coefficients in the model pore are ~400-fold (Na) or ~5000-fold (Ca) smaller than coefficients measured in dilute solutions. Both the larger disparity and the small magnitude of the diffusion coefficients suggest that diffusion in the pore is limited by factors that differ markedly from those in dilute bulk solutions. Very concentrated solutions of many salts exhibit a substantial decrease in conductivity with increasing concentration, and these solutions have an increased viscosity (Robinson and Stokes, 1959, Chap. 11). The Ca-supported conductivity of the pore (0.03 S/m) is in a range observed for solid salts at temperatures slightly below their

melting points (Ashcroft and Mermin, 1976, Chap. 30). Thus the diverse excess chemical affinities and the diverse diffusion coefficients for Ca and Na ions all could originate from strong electrostatic interactions among structural and mobile charges in the Ca channel.

CONCLUSION

A Poisson-Nernst-Planck theory (PNP2) predicts many conduction properties of the open L-type Ca channel as electrostatic consequences of negatively charged carboxyl groups in the pore lining. Selectivity in this channel is in part a consequence of ionic valence, but it also involves diffusion coefficients and excess chemical potentials that are different for different ions. These additional ion-specific effects resemble behaviors of highly concentrated salt solutions and thus might be computed in the future from modern electrochemical theories of such solutions. PNP2 computes conduction as average ion flow in a field of mean force. A concise description of Ca channel conduction is obtained without the need to reconstruct individual ion trajectories in atomic detail. PNP2 seems a useful first-order theory of ion channel selectivity as well as conduction.

APPENDIX

This appendix examines energy profiles for a model of the L-type Ca channel that predicts ion channel selectivity through stepwise changes in binding affinity (Dang and McCleskey, 1998). This model is based on the rate theory analysis of Hille and Schwarz (1978), and was published after the present work was submitted. Here we compute currents predicted to flow across these energy profiles, using the PNP2 theory described in the body of this paper. The currents computed with PNP2 differ substantially from those computed with rate theory, and thus also differ from the experimentally observed currents that the step model seeks to reproduce. These results are presented at the suggestion of the reviewers and may be of general interest beyond L-type Ca channels.

Rate theory models of permeation describe the diffusion of ions through an ion channel as a succession of jumps over energy barriers separated by energy wells (Hille and Schwarz, 1978). Interactions between the permeating ions and atoms of the channel and water are defined by this energy profile. Interactions between the ions in the pore are described by ad hoc repulsion factors, and the transmembrane voltage only tilts the energy profile. These models are an approximate description of a complex diffusion process, but it is not clear how large the errors are for a specific channel. As far as we know, no direct comparison has been made between this rate theory treatment and a more rigorous treatment of the permeation process in the traditions of electrostatics and chemical kinetics.

In the PNP2 theory, ion movement is instead treated as diffusion across profiles of electrochemical potential that can represent any configuration of barriers and wells. Friction is included in the form of diffusion coefficients. The electric field is computed by solving Poisson's equation, including both the structural charge assigned to the channel and the mobile charge of ions present in and around the pore. By simultaneously solving the Nernst-Planck and Poisson equations, PNP2 predicts the concentration and electric potential profiles in the presence of flux.

We analyzed the step model as defined in Fig. 1 of Dang and McCleskey (1998). The energy profiles for this model exclude electrostatic interactions between Na and Ca ions, but include (electrostatic and other) ion/pore interactions. We imported the energy profiles of this model into a PNP2 formulation as excess chemical potentials, $\mu^0_{Ca}(x)$ and $\mu^0_{Na}(x)$. Because all ion/pore interactions were thereby described as chemical potentials, the structural charge in PNP2 was set to zero. No assumptions were made about the electrostatic interactions among mobile ions in the pore: these were computed from Poisson's equation and the ion concentrations. Because the step model includes no reference to the dimensions of the pore, we used the dimensions described in Fig. 1, assuming that the electric coordinates of the step model apply to the pore proper. In the absence of a specification for frictional effects, we assigned Na, Ca, and Cl ions in the pore the diffusion coefficients measured in dilute aqueous bulk solutions. The step model excludes anions from the pore by definition. We assigned Cl ions a large repulsive chemical potential (0.3 eV, equivalent to $\sim 12kT$) throughout the pore proper, which is likely to reduce the concentration of chloride in the pore (and thus its conductance) by $e^{12} = 1.6 \times 10^5$.

Fig. 11 *A* plots current-voltage relationships computed via PNP2 with

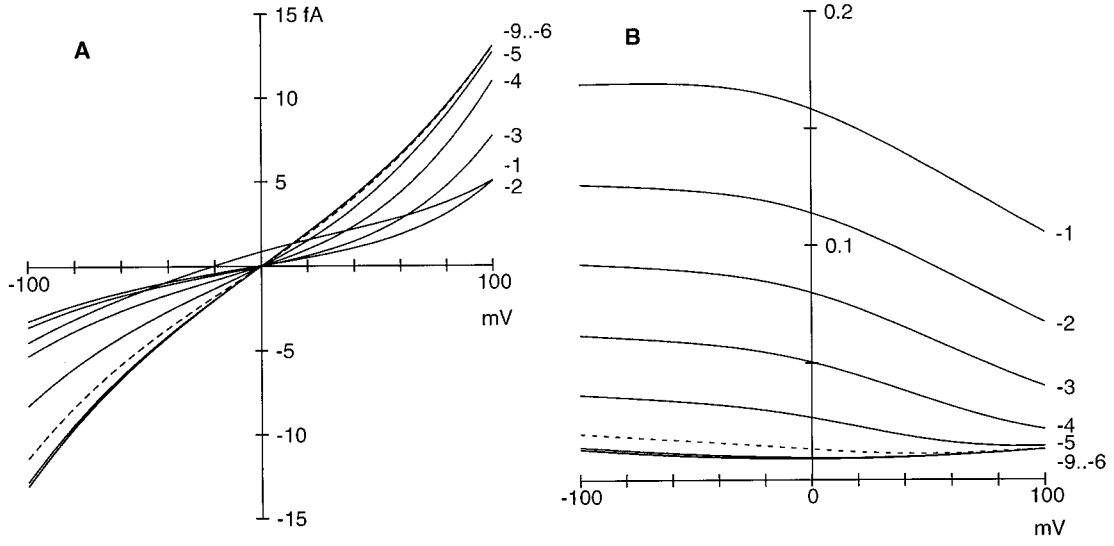

FIGURE 11 Predictions for the step model: current/voltage curves (*A*) and ionic occupancies (*B*) at various extracellular Ca concentrations. The solutions contained symmetrical 100 mM NaCl. $CaCl_2$ was added to only the extracellular solution in 10-fold increments from 10^{-9} to 10^{-1} M (the curves are labeled by the exponent of the power of 10, e.g., -9 for 10^{-9}; the curves for 10^{-6} M are plotted as *dashed lines*). Occupancies give the average number of ions (sum of Na, Ca, and Cl) present in the pore proper.

the barrier-and-well profile of the step model. The ionic conditions used are similar to those of Figs. 3 and 4 in the body of this paper: 100 mM symmetrical NaCl with $CaCl_2$ concentrations added as indicated to the extracellular side. The computed currents for the step model are many hundredfold smaller than those observed experimentally, even though friction is likely to be underestimated in our computation because of the use of bulk diffusion coefficients in the pore.

The rate theory method computes currents of appropriate magnitude from this energy profile because it scales rate constants with the large prefactor, kT/h ($\sim 6 \times 10^{12}$/s), which does not account for friction due to collisions between ions and neighboring atoms in the pore. Prefactors that do account for friction are several (2–4) orders of magnitude smaller than kT/h (see Appendix in Chen et al., 1997b). If the diffusion prefactor is used, barrier energies must be much lower than those used in the rate theory model, if they are to give appropriate rate constants. Transport across such small energy barriers cannot be computed with the high-barrier approximation used in rate theory, but is appropriately treated as diffusion across an energy profile (as is done in PNP2). When the ion barriers of the step model are reduced from $10kT$ to $1kT$ (while diffusion coefficients are kept equal to those in bulk solution), the computed Na currents are nevertheless smaller than those observed experimentally. The small currents reflect the very low ionic occupancy of the pore produced by the energy profile of the step model, as we show below. The concentration of charge carriers is insufficient to support the experimentally observed currents, even when barriers are virtually eliminated from the profile, and diffusion coefficients are overestimated by using their values in bulk solutions.

The PNP2 computations with the step model energy profile do not predict the selectivity pattern of the L-type Ca channel (Fig. 11 *A*). The predicted reversal potential is close to zero for all external $CaCl_2$ concentrations up to 10 mM, and changes to ~ -20 mV at 100 mM $CaCl_2$. The step model channel mostly conducts Na ion when Ca concentration is very low, and this Na flux is reduced as Ca is increased to the micromolar range. An increase of Ca to the millimolar range, however, does not produce a significant Ca flux that could affect the reversal potential. When the external solution contains 100 mM $CaCl_2$, Cl ion becomes the dominant charge carrier, whereas Na flux is reduced further. Thus the step model channel does not reveal any sign of selectivity for Ca over Na; instead the step model channel selects for Cl over cations! This, despite the $12kT$ of energy used to exclude Cl ions from the pore.

Fig. 12 plots electric potential and concentration profiles for the step model when the transmembrane potential is zero. At 100 mM external Ca, a high concentration of Ca is bound in the center of the pore (Fig. 12 *C*). The excess positive charge associated with the bound Ca ion is sufficient to create a large positive potential (up to ~110 mV) that extends from the center of the pore beyond the edges of the pore proper (Fig. 12 *A*). The lateral regions are depleted of Ca (and Na) ions by the large positive electrostatic potential and the chemical potential assigned to the outer barriers. Hence they become regions of low Ca and Na conductance. This kind of depletion phenomenon, which results from strong chemical binding of ions, is discussed in Nonner et al. (1998). The depletion effect by a positive electric potential is stronger for divalent Ca than for monovalent Na, and thus Ca conductance is even more depressed than Na conductance.

In effect, the very high Ca affinity of the step model pore prevents the selective conduction of Ca. The positive space charge created by bound Ca helps attract Cl ions to the pore (Fig. 12 *D*) and allows them to pass, even if Cl ions experience a strong chemical potential ($\sim 12kT$) that tends to repel them from the pore. The electrostatics dominate.

PNP2 theory predicts that the mean number of ions present in the step model of the Ca channel is smaller by more than an order of magnitude than that predicted in the rate theory computations. Fig. 11 *B* plots the mean number of ions in the pore proper (Ca, Na, and Cl together). This number is less than 0.2 for the range of conditions examined in Fig. 11 *A*, as compared to the rate-theory computations, which gave mean occupancies greater than 2 for Ca at high external concentrations. The predictions also show that Ca does not significantly occupy either of the exterior energy wells, even at 100 mM concentration (Fig. 12 *C*), because the electrostatic repulsion overcomes the binding energy due to the chemical potential.

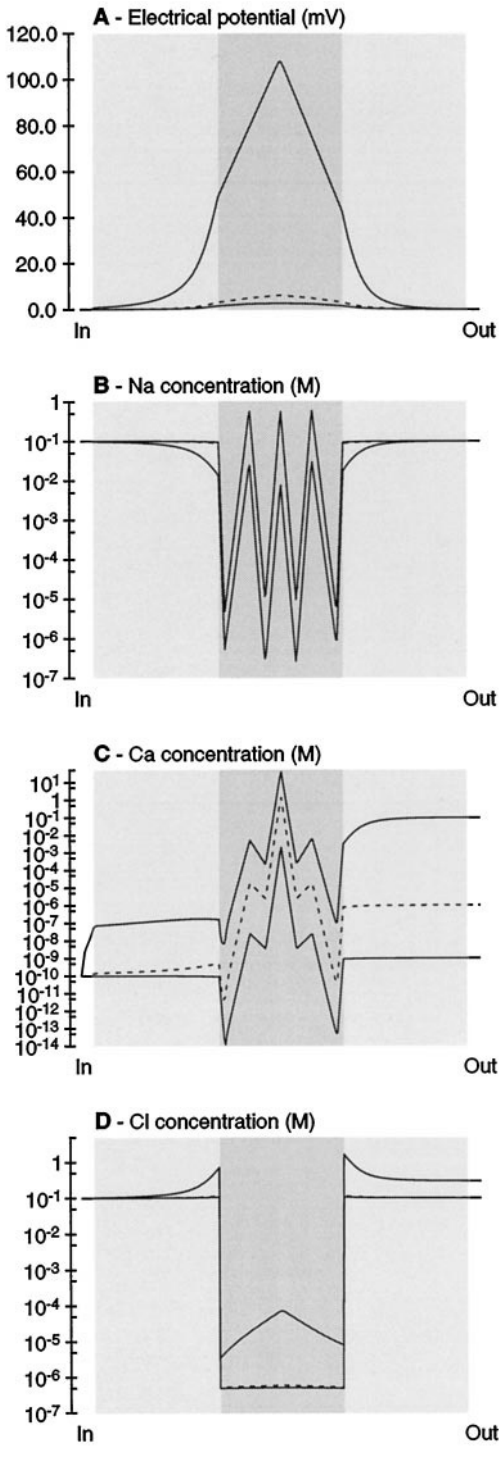

FIGURE 12 Profiles of electric potential and Na, Ca, and Cl ion concentrations as functions of bulk extracellular [$CaCl_2$]. These profiles correspond to the *I/V* relationships plotted in Fig. 11 *A*; only the curves corresponding to 10^{-9}, 10^{-6} (*dashed lines*), and 10^{-1} M Ca are shown for clarity. The transmembrane potential was 0 mV. The abscissa is nonlinear; the bulk section (*white background*) and atrial sections (*light gray*) are compressed 100- or 2-fold compared to the pore proper (*darker gray*). Actual dimensions are given in the body of the paper.

The predicted Ca selectivity is even less consistent with that experimentally observed when we use the energy profiles of the repulsion model of Hess and Tsien (1984) and Almers and McCleskey (1984) (not shown).

In summary, neither of the previously proposed models (step or repulsion) of the L-type Ca channel predicts the experimentally observed currents if these models are evaluated with a self-consistent computation of electrostatics and friction. The reasons for the failure of these models are generic for rate theory models in the tradition of Hille and Schwarz (1978), which describe electrostatics by ad hoc repulsion factors and do not account for the friction involved in reactions in the condensed phase. Because these rate theory models violate Coulomb's law, they imply the existence of unstated sources of charge and energy. Literature concerning appropriate methods for analyzing friction is cited in Chen et al. (1997b, Appendix). Appropriate methods for computing the electric field, which include that used in this work, can be found in Abraham's classical *Theory of Electricity* (1904; translated and revised in Becker, 1964).

It is a pleasure to thank Drs. Ellen Barrett, Karl Magleby, Chris Miller, and Luigi Catacuzzeno for their most useful comments on drafts of the manuscript. We are fortunate that Dr. Lesser Blum has helped us learn some modern electrochemistry.

This work was supported by National Institutes of Health grant GM30377 (to WN) and grants from the National Science Foundation and Defense Advanced Research Projects Agency (to BE).

REFERENCES

Almers, W., and E. W. McCleskey. 1984. Non-selective conductance in calcium channels of frog muscle: calcium selectivity in a single-file pore. *J. Physiol. (Lond.)*. 353:585–608.

Almers, W., E. W. McCleskey, and P. T. Palade. 1984. A non-selective cation conductance in frog muscle membrane blocked by micromolar external calcium ions. *J. Physiol. (Lond.)*. 353:565–583.

Armstrong, C. M., and J. Neyton. 1992. Ion permeation through Ca channels. A one-site model. *Ann. N.Y. Acad. Sci.* 635:18–25.

Ashcroft, N. W., and N. D. Mermin. 1976. Solid State Physics. Holt, Rinehard and Winston, New York.

Barcilon, V. 1992. Ion flow through narrow membrane channels. Part I. *SIAM J. Appl. Math.* 52:1391–1404.

Barkai, E., R. S. Eisenberg, and Z. Schuss. 1996. A bidirectional shot noise in a singly occupied channel. *Phys. Rev. E(2).* 54:1161–1175.

Becker, R. 1964. Electromagnetic Fields and Their Interactions. Dover reprint of Blaisdell Publishing, New York.

Bernard, O., and L. Blum. 1996. Binding mean spherical approximation for pairing ions: an exponential approximation and thermodynamics. *J. Chem. Phys.* 104:4746–4754.

Blum, L. 1975. Mean spherical model for asymmetric electrolytes. I. Method of solution. *Mol. Biophys.* 30:1529.

Blum, L., and J. S. Hoye. 1977. Mean spherical approximation for asymmetrical electrolytes. II. Thermodynamic properties and the pair correlation function. *J. Phys. Chem.* 81:1311–1316.

Brooks, C. L., M. Karplus, and B. M. Pettitt. 1988. Proteins: A Theoretical Perspective of Dynamics, Structure and Thermodynamics. John Wiley and Sons, New York.

Chen, D. P. 1997. Nonequilibrium thermodynamics of transports in ion channels. *In* Progress of Cell Research: Towards Molecular Biophysics of Ion Channels. M. Sokabe, A. Auerbach, and F. Sigworth, editors. Elsevier, Amsterdam. 269–277.

Chen, D. P., and B. Eisenberg. 1993. Charges, currents and potentials in ionic channels of one conformation. *Biophys. J.* 64:1405–1421.

Chen, D. P., J. Lear, and R. S. Eisenberg. 1997a. Permeation through an open channel. Poisson-Nernst-Planck theory of a synthetic ionic channel. *Biophys. J.* 72:97–116.

Chen, D., L. Xu, A. Tripathy, G. Meissner, and R. Eisenberg. 1997b. Permeation through the calcium release channel of cardiac muscle. *Biophys. J.* 73:1337–1354.

Chen, X. H., I. Bezprozvanny, and R. W. Tsien. 1996. Molecular basis of proton block of L-type Ca^{2+} channels. *J. Gen. Physiol.* 108:363–374.

Creighton, T. E. 1984. Proteins: Structures and Molecular Properties. W. H. Freeman and Company, New York. 7.

Dang, T. X., and E. W. McCleskey. 1998. Ion channel selectivity through stepwise changes in binding affinity. *J. Gen. Physiol.* 111:185–193.

Dani, J. A. 1986. Ion-channel entrances influence permeation. Net charge, size, shape, and binding considerations. *Biophys. J.* 49:607–618.

Das, S., U. D. Lengweiler, D. Seebach, and R. N. Reusch. 1997. Proof for a nonproteinaceous calcium-selective channel in *Escherichia coli* by total synthesis from (R)-3-hydroxybutanoic acid and inorganic polyphosphate. *Proc. Natl. Acad. Sci. USA.* 94:9075–9079.

Ellinor, P. T., J. Yang, W. A. Sather, J. F. Zhang, and R. W. Tsien. 1995. Ca^{2+} channel selectivity at a single locus for high-affinity Ca^{2+} interactions. *Neuron.* 15:1121–1132.

Eisenberg, R. S. 1996. Computing the field in proteins and channels. *J. Membr. Biol.* 150:1–25.

Eisenman, G., R. Latorre, and C. Miller. 1986. Multi-ion conduction and selectivity in the high-conductance Ca^{++}-activated K^+ channel from skeletal muscle. *Biophys. J.* 50:1025–1034.

Heinemann, S. H., H. Terlau, W. Stühmer, K. Imoto, and S. Numa. 1992. Calcium channel characteristics conferred on the sodium channel by single mutations. *Nature.* 356:441–443.

Helfferich, F. 1962. Ion Exchange. McGraw-Hill, New York.

Hess, P., J. F. Lansman, and R. W. Tsien. 1986. Calcium channel selectivity for divalent and monovalent cations. *J. Gen. Physiol.* 88:293–319.

Hess, P., and R. W. Tsien. 1984. Mechanism of ion permeation through calcium channels. *Nature.* 309:453–456.

Hille, B., and W. Schwarz. 1978. Potassium channels as multi-ion single-file pores. *J. Gen. Physiol.* 72:409–442.

Hoye, J. S., and L. Blum. 1978. Addenda to the mean spherical approximation for asymmetrical electrolytes: thermodynamics and the pair correlation function. *Mol. Phys.* 35:299–300.

Jordan, P. C., R. J. Bacquet, J. A. McCammon, and P. Tran. 1989. How electrolyte shielding influences the electric potential in transmembrane ion channels. *Biophys. J.* 55:1041–1052.

Kim, M. S., T. Mori, L. X. Sun, K. Imoto, and Y. Mori. 1993. Structural determinants of ion selectivity in brain calcium channel. *FEBS Lett.* 318:145–148.

Lansman, J. B., P. Hess, and R. W. Tsien. 1986. Blockade of current through single calcium channels by Cd^{2+}, Mg^{2+}, and Ca^{2+}. Voltage and concentration dependence of calcium entry into the pore. *J. Gen. Physiol.* 88:321–347.

Lee, K. S., and R. W. Tsien. 1983. High selectivity of calcium channels in single dialysed heart cells of the guinea-pig. *J. Physiol. (Lond.)*. 354: 253–272.

McCleskey, E. W., and W. Almers. 1985. The Ca channel in skeletal muscle is a large pore. *Proc. Natl. Acad. Sci. USA.* 82:7149–7153.

Mikala, G., A. Bahinski, A. Ytani, S. Tang, and A. Schwartz. 1993. Differential contribution of conserved glutamate residues to an ion-selectivity site in the L-type Ca^{2+} channel pore. *FEBS Lett.* 335: 265–269.

Mikami, A., K. Imoto, T. Tanabe, T. Niidome, Y. Mori, H. Takeshima, S. Narumiya, and S. Numa. 1989. Primary structure and functional expression of the cardiac dihydropyridine-sensitive calcium channel. *Nature.* 340:230–233.

Nonner, W., D. P. Chen, and B. Eisenberg. 1998. Anomalous mole fraction effect, electrostatics, and binding in ionic channels. *Biophys. J.* 74: 2327–2334.

Peskoff, A., and D. M. Bers. 1988. Electrodiffusion of ions approaching the mouth of a conducting membrane channel. *Biophys. J.* 53:863–875.

Pietrobon, D., B. Prod'hom, and P. Hess. 1989. Interactions of protons with single open L-type calcium channels. *J. Gen. Physiol.* 94:1–21.

Prod'hom, B., D. Pietrobon, and P. Hess. 1989. Interactions of protons with single open L-type calcium channels. Location of protonation site and dependence of proton-induced current fluctuations on concentration and species of permeant ion. *J. Gen. Physiol.* 94:23–42.

Reusch, R. N., R. Huang, and L. L. Bramble. 1995. Poly-3-hydroxybutyrate/polyphos phate complexes form voltage-activated Ca^{2+} channels in the plasma membranes of *Escherichia coli*. *Biophys. J.* 69:754–766.

Robinson, R. A., and R. H. Stokes. 1959. Electrolyte Solutions. Butterworths Scientific Publications, London.

Romano, J. D., and R. H. Price. 1996. The conical resistor conundrum: a potential solution. *Am. J. Phys.* 64:1150–1153.

Tanabe, T., H. Takeshima, A. Mikami, V. Flockerzi, H. Takahashi, K. Kangawa, M. Kojima, H. Matsuo, T. Hirose, and S. Numa. 1987. Primary structure of the receptor for calcium channel blockers from skeletal muscle. *Nature.* 328:313–318.

Teorell, T. 1953. Transport processes and electrical phenomena in ionic membranes. *Prog. Biophys. Mol. Biol.* 3:305–369.

Tsien, R. W., P. Hess, E. W. McClesky, and R. L. Rosenberg. 1987. Calcium channels: mechanisms of selectivity, permeation, and block. *Annu. Rev. Biophys. Biophys. Chem.* 16:265–290.

Wilmer, D., T. Kantium, O. Lamberty, K. Funke, M. D. Ingram, and A. Bunde. 1994. Electrical and mechanical mixed alkali effect in a Li/Na borate glass at gigahertz frequencies. *Solid State Ionics.* 70–71:323.

Yang, J., P. T. Ellinor, W. A. Sather, J. Zhang, and R. W. Tsien. 1993. Molecular determinants of Ca^{2+} selectivity and ion permeation in L-type Ca^{2+} channels. *Nature.* 366:158–161.